# First-principles demonstration of superconductivity at 280 K in hydrogen sulfide with low phosphorus substitution

Yanfeng Ge,[1] Fan Zhang,[2,*] and Yugui Yao[1,†]
[1]*School of Physics, Beijing Institute of Technology, Beijing 100081, China*
[2]*Department of Physics, University of Texas at Dallas, Richardson, Texas 75080, USA*
(Received 4 October 2015; revised manuscript received 18 May 2016; published 16 June 2016)

Recently, BCS superconductivity at 203 K has been observed in a highly compressed hydrogen sulfide. We use first-principles calculations to systematically examine the effects of partially substituting chalcogen atoms on the superconductivity of hydrogen chalcogenides under high pressures. We find detailed trends of how the critical temperature changes upon increasing the V-, VI- or VII-substitution rate. These trends highlight the key roles played by low atomic mass and metallized covalent bonds. In particular, a possible record high critical temperature of 280 K is predicted in stable $H_3S_{0.925}P_{0.075}$ with the $Im\bar{3}m$ structure under 250 GPa.

DOI: 10.1103/PhysRevB.93.224513

## I. INTRODUCTION

Since the discovery of superconductivity in mercury at 4 K in 1911 [1], scientists have been ardently pursuing new and better superconductors at higher temperatures. In a conventional superconductor, the vibrations of a crystal lattice provide an attractive force that binds an electron with its time-reversal partner into a Cooper pair [2]. The Cooper pairs can Bose-condense below a critical temperature ($T_c$), which had been believed to be no larger than 25 K prior to the discovery of $MgB_2$ [3,4]. In this case, the Debye temperature could be as large as $\sim 10^3$ K, and low $T_c$ is primarily related to small electron-phonon couplings [5]. Since 1986 and 2008, respectively, the discoveries of copper- and iron-based superconductors have provided two new avenues for making high-$T_c$ superconductors [6–12] while generating new interest in fundamental physics. Although their unconventional mechanisms are still under debate, to date a record $T_c$ of 164 K has been experimentally realized in the cuprate family [9] and 56 K among the iron-pnictide compounds [12].

One may thus wonder whether a $T_c$ higher than 164 K could be achieved and whether the conventional phonon-mediated mechanism could play a significant role in such a race. Both answers have become extremely positive and fascinating, given the prediction [13] of superconductivity in highly compressed hydrogen sulfide $H_3S$ [14] and particularly the most recent experimental observation [15,16] of superconductivity at 203 K [13–23]. As pointed out by Bernstein *et al.* in a microscopic theory of $H_3S$ [17], the strong covalent metallic nature leads to a large electron-phonon coupling, and the low atomic mass leads to high-frequency phonon modes. Both features play essential roles in increasing the $T_c$ of $H_3S$. Notably, the former feature is analogous to that of $MgB_2$ [24,25], whereas the latter effect is similar to those in the H-rich materials [26–38].

As a powerful method for the optimization of $T_c$, the atomic substitution has been routine in superconductivity experiments [39–42]. However, there has yet to be any study on how the atomic substitution influences the $T_c$ of $H_3S$ and of the more general hydrogen chalcogenides. Here, we systematically examine the effects of (partially) substituting the chalcogen atoms on the superconductivity and particularly the $T_c$'s of hydrogen chalcogenides in the $Im\bar{3}m$ phase under high pressures, based on the first-principles calculations with the virtual crystal approximation (VCA) [43–47]. In the V- and VII-substitution cases, we find that the significant changes of the density of states (DOS) at the Fermi surface and of the phonon linewidths, coming from the different number of valance electrons, are the principal factors affecting the electron-phonon coupling and $T_c$. In the particular case of $H_3S_{1-x}P_x$ at 200 GPa, we find that the DOS, the electron-phonon coupling constant, and the $T_c$ all first increase and then decrease as the P-substitution rate increases from zero to 0.2. In the optimized condition in which $x = 0.075$ and the pressure increases to 250 GPa, a possible record high $T_c$ of 280 K is predicted. In contrast, the $T_c$ decreases monotonously with increasing the VII-substitution degree. In the VI-substitution cases, the $T_c$ does not appear to increase substantially because of the reduction of the DOS with O- or Se-substitution, or due to the softening of the logarithmically averaged phonon frequency with Te-substitution. These findings emphasize the importance of low atomic mass and metallized covalent bonds in conventional high-$T_c$ superconductors, they pave the way for substantially enhancing $T_c$ by combining application of a high pressure and properly designed chemical substitution, and they suggest that in principle it is not impossible to boost $T_c$ to the ice point in optimized conditions.

Our paper is organized as follows. In Sec. II, we first introduce our computational methods. We then discuss our results in V-, VI-, and VII-substitution systems in Secs. III and IV, followed by the pressure effects in Sec. V and several discussions in Sec. VI. The Appendixes provide the important but technical details.

## II. METHODS

Soon after the experimental report [15,16] on the record $T_c$ of a highly compressed hydrogen sulfide [13,14], further theoretical studies [17–23] reached two consensuses: (i) the superconducting matter is most likely $H_3S$ with a strong covalent character in the $Im\bar{3}m$ phase, as sketched in Fig. 1(a),

*zhang@utdallas.edu
†ygyao@bit.edu.cn

 

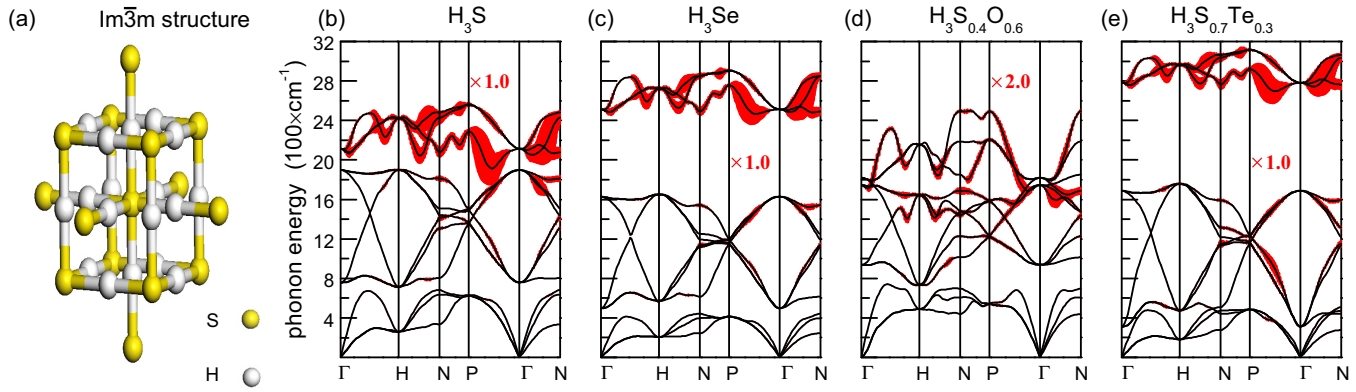


FIG. 1. $Im\bar{3}m$ structure of $H_3S$ and phonon spectra with a phonon linewidth of VI-substitution systems at 200 GPa. (a) The $Im\bar{3}m$ structure of hydrogen chalcogenides. (b)–(e) Phonon spectra and phonon linewidths of four representative VI-substitution systems: (b) $H_3S$, (c) $H_3Se$, (d) $H_3S_{0.4}O_{0.6}$, and (e) $H_3S_{0.7}Te_{0.3}$. The magnitude of the phonon linewidth is indicated by the size of the red error bar, and the magnitude for $H_3S_{0.4}O_{0.6}$ is plotted with twice the real values.

and (ii) the superconductivity of $H_3S$ is phonon-mediated. Note that the $Im\bar{3}m$ phase has already been confirmed by a recent x-ray experiment [48]. Thus, the superconductivity of highly compressed hydrogen sulfide can be accurately described by the celebrated Eliashberg theory [49], which takes into account the renormalization of electron-electron repulsion by electron-phonon interactions. In this theory, the Allen-Dynes-modified McMillan formula [50,51] relates $T_c$ to the logarithmically averaged phonon frequency $\omega_{\ln}$, the effective Coulomb repulsion $\mu^*$, and the electron-phonon coupling constant $\lambda$:

$$T_c = f_1 f_2 \frac{\omega_{\ln}}{1.20} \exp\left[-\frac{1.04(1+\lambda)}{\lambda - \mu^*(1+0.62\lambda)}\right], \quad (1)$$

where $f_1$ and $f_2$ are the strong coupling and the shape correction factors [50], respectively. More details on the McMillan formula are given in Appendix A.

Clearly, there are two ways to enhance $T_c$, i.e., to search for materials with high-frequency phonon modes and to increase electron-phonon couplings. As mentioned in the Introduction, the $H_3S$ happens to constitute both advantages and hence has a record high $T_c$. Indeed, within this framework recent theoretical calculations have well explained the high $T_c$ in the highly compressed hydrogen sulfide [13–23,52]. Therefore, we will first reproduce the $T_c$ of $H_3S$ in the $Im\bar{3}m$ phase at 200 GPa and study the substitution of S atoms by other VI atoms. Comparing our results with previous ones will show the validity of our first-principles calculations with the virtual crystal approximation (VCA).

There are mainly two different procedures for disordered systems and partial atomic substitutions in first-principles calculations, i.e., an ordered supercell and the VCA [43]. The former method is time-consuming and technically difficult to deal with in the case of small concentrations. Thus, we chose to use the VCA in this work. To benchmark the validity of the VCA in the present work, in Appendix E we have compared the VCA and the supercell method for the special case of $H_3S_{0.875}P_{0.125}$. In calculations based on the VCA, the primitive periodicity is retained but composed of virtual atomic potentials interpolating between the behaviors of actual components. Even though this approach neglects the local deformations around atoms and cannot explore the disordered structures very accurately, it often produces acceptable and useful results that have been verified in many research fields of condensed-matter physics [42,44–47,53–58]. The atomic substitution in the present work is simulated by the self-consistent VCA. For example, in $H_3S_{1-x}Se_x$ the virtual pseudopotentials of $S_{1-x}Se_x$ are represented by a pseudopotential operator $V_{\rm VCA} = xV_{\rm Se} + (1-x)V_{\rm S}$, where $V_{\rm Se}$ ($V_{\rm S}$) is the pseudopotential of the Se (S) atom.

The present studies, including the electronic structures, the phonon spectra, and the electron-phonon couplings, were carried out using the ABINIT package [59–62] with the local-density approximation (LDA). Hartwigsen-Goedecker-Hutter (HGH) pseudopotentials [63] were used in order to include spin-orbit couplings (SOCs) for the heavy element, tellurium. The SOCs for other elements were neglected since they are sufficiently light. By requiring convergence of results, the kinetic-energy cutoff of 30 Hartree and the Monkhorst-Pack $k$-mesh of $40 \times 40 \times 40$ were used in all calculations dealing with the electronic ground-state properties. The phonon spectra and the electron-phonon couplings were calculated on an $8 \times 8 \times 8$ $q$-grid. Since calculating electron-phonon couplings referred to integrals over the Brillouin zone, we also carefully checked convergence of the results on the aforementioned $k$-mesh and $q$-grid by comparing them with results in denser samples (a $40 \times 40 \times 40$ $k$-mesh and a $10 \times 10 \times 10$ $q$-grid).

## III. VI-SUBSTITUTION SYSTEMS

In the VI-substitution systems at 200 GPa, we focus on studying $H_3S_{1-x}Se_x$ in the full range of $x$, $H_3S_{1-x}O_x$ in the range of $x = 0.0$–$0.6$, and $H_3S_{1-x}Te_x$ in the range of $x = 0.0$–$0.3$. This is because when $x$ takes a greater value in the case of O- or Te-substitution, we can find imaginary phonon modes at the $\Gamma$ point, indicating a lattice structure instability. The electronic band structures of these systems are shown in Appendix B, and our results for $H_3S$ and $H_3Se$ are in qualitative agreement with previous reports based on similar first-principles calculations [14,64,65]. We find that the VI-substitutions have little influence on the electronic band structure around the Fermi energy, except for some unimportant

TABLE I. Fermi-surface DOS (in units of Hartree$^{-1}$/spin) of hydrogen chalcogenides in various V-, VI-, and VII-substitution systems at 200 GPa.

| $x$ | $H_3S_{1-x}O_x$ | $H_3S_{1-x}Se_x$ | $H_3S_{1-x}Te_x$ | |
|---|---|---|---|---|
| 0.0 | 7.91 | 7.91 | 7.91 | |
| 0.1 | 7.70 | 7.78 | 7.90 | |
| 0.3 | 6.84 | 7.61 | 7.53 | |
| 0.6 | 4.53 | 7.51 | | |
| 1.0 | | 7.31 | | |
| $x$ | $H_3S_{1-x}P_x$ | $H_3Se_{1-x}As_x$ | $H_3S_{1-x}Cl_x$ | $H_3Se_{1-x}Br_x$ |
| 0.000 | 7.91 | 7.31 | 7.91 | 7.31 |
| 0.025 | 8.57 | 7.80 | 7.18 | 6.50 |
| 0.050 | 9.11 | 7.79 | 6.58 | 5.85 |
| 0.075 | 9.92 | 7.90 | 5.63 | 5.23 |
| 0.100 | 10.55 | 7.96 | 5.02 | 4.72 |
| 0.125 | 9.21 | 8.27 | 4.84 | 4.55 |
| 0.150 | 8.02 | 8.38 | 4.71 | 4.39 |
| 0.175 | 7.22 | 8.12 | 4.59 | 4.25 |
| 0.200 | 6.69 | 6.92 | 4.47 | 4.14 |

changes near Γ point (see Appendix B). We further find that including spin-orbit couplings for the Te-substitution case does not introduce any significant correction either. Notably, the main electronic effect is the reduction of the DOS at the Fermi surface in all of these VI-substitution cases, as summarized in Table I. The DOS decreases monotonically upon increasing the VI-substitution rate. Moreover, the lighter the substitution element, the stronger the reduction of the DOS.

Figures 1(b)–1(e) display the phonon spectra of four representative VI-substitution systems, and the magnitude of the phonon linewidth is indicated by the size of the red error bar. Note that our LDA results and previous GGA results [19,65] have appreciable but inessential differences on $H_3S$ and $H_3Se$, which arise mainly from the different exchange-correlation functions and program codes [66]. Overall there is a clear separation between H modes at high energy and S modes at low energy [19]. Evidently, upon increasing the degree of heavy-element (Se or Te) substitution, all three acoustic phonon modes decrease in frequency. In addition, the H-VI bond-bending modes (displacement of an H atom perpendicular to a H-VI bond) in the intermediate frequency region are softened, whereas the H-VI bond-stretching modes (displacement of an H atom parallel to a H-VI bond) in the high-frequency region are hardened. Not surprisingly, the opposite trends occur for the case of O-substitution. The above changes at low and intermediate frequency are expected by considering the relative atomic mass of the substitution elements, whereas the changes at high frequency might be explained by the dependence of the chemical precompression effect [27,65,67] on the atomic radius of VI elements.

Further analyzing phonon linewidths reveals that they are larger for the H vibrational modes, particularly for the bond-stretching modes at high frequency, similar to the results by Errea *et al.* [19]. We note that the small magnitude of the phonon linewidth in $H_3S_{0.4}O_{0.6}$ [Fig. 1(d)] is ascribed to the reduction of the DOS. To expose more clearly the relative contributions of different phonon modes to the electron-phonon coupling constant λ, we define an integral function $\lambda'(\omega) = 2\int_0^{\omega} \omega'^{-1}\alpha^2F(\omega')d\omega'$, where $\lambda'(\infty)$ is λ and $\alpha^2F(\omega)$ is the Eliashberg function [68–70]. As shown in Fig. 2(a), the contribution from the intermediate frequency region (300–1700 cm$^{-1}$) has an increase in $H_3S_{0.7}Te_{0.3}$, which results in a corresponding increase in the electron-phonon coupling constant. Such a variation is a consequence of the increase of phonon linewidths in the intermediate-frequency region, which is present in Fig. 1(e) but absent in the O- and Se-substitution systems [Figs. 1(c) and 1(d)].

With the above results, we use Eq. (1) to estimate the $T_c$ for the investigated VI-substitution systems, and the results

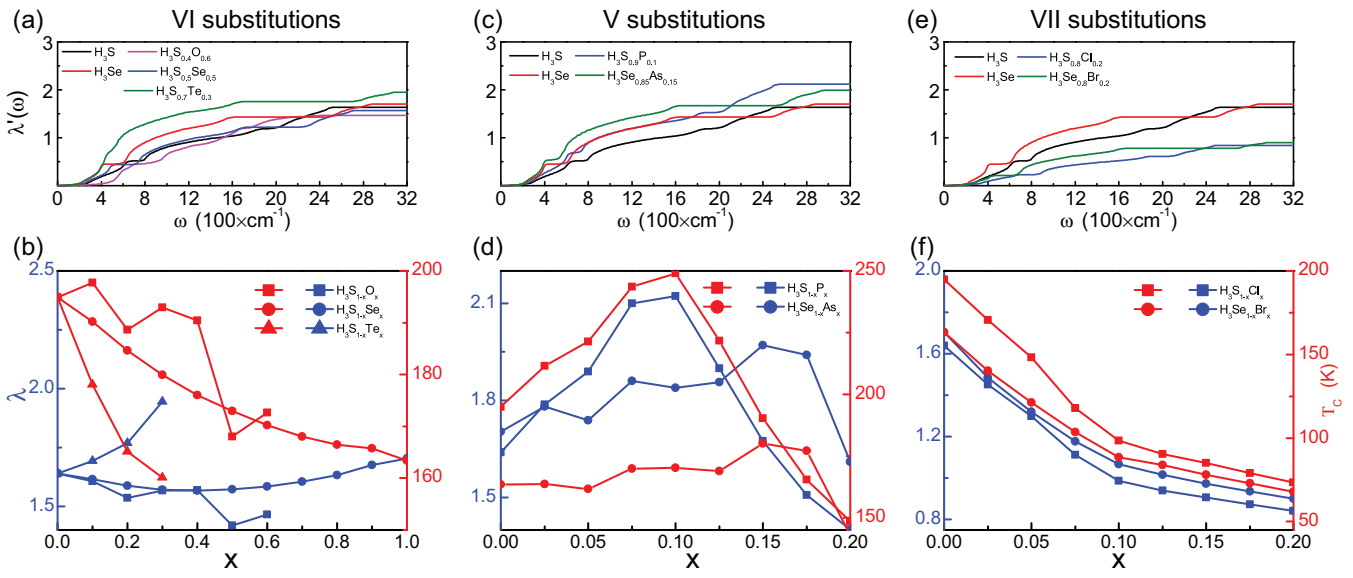


FIG. 2. Electron-phonon coupling and critical temperature at 200 GPa of hydrogen chalcogenides with chemical substitutions. Upper panels: the integral function $\lambda'(\omega)$. Lower panels: the electron-phonon coupling constant λ (blue lines) and the critical temperature $T_c$ (red lines) vs the substitution concentration $x$. The left, middle, and right panels show the results for the case of VI-, V-, and VII-substitutions, respectively.

are plotted in Fig. 2(b). The effective Coulomb repulsion has been chosen to be $\mu^* = 0.12$, in the reasonable range of 0.1–0.15 [71], such that the estimated $T_c$ for $H_3S$ and $H_3Se$, 194 and 160 K, are closest to the reported values [19,64]. In all of the VI-substitution cases, there is no substantial enhancement of $T_c$ compared with the 194 K in $H_3S$, except a slightly higher $T_c$ of 198 K in $H_3S_{0.9}O_{0.1}$. Notably, despite a higher $\lambda$ in $H_3S_{0.7}Te_{0.3}$, the $T_c$ is in fact reduced to 161 K. Because of the heavy mass of Te, the logarithmically averaged phonon frequency $\omega_{\ln}$ is only 90.8 meV in $H_3S_{0.7}Te_{0.3}$, much lower than the 125.2 meV in $H_3S$. In fact, the effect of VI-substitution at a fixed physical pressure can be viewed as a chemical pressure effect. Thus, our results that the $T_c$ would decrease in the various VI-substitution cases at 200 GPa are in agreement with the experimental observation [16] and an earlier theoretical study [21], which have confirmed that the $T_c$ of $H_3S$ is peaked near 200 GPa.

## IV. V- AND VII-SUBSTITUTION SYSTEMS

In addition to the substitution of S by elements in the same main group, we also further consider substitutions by the adjacent group elements, i.e., phosphorus and halogen groups. We mainly focus on the cases in which a small percentage ($x = 0.0$–$0.2$) of S is replaced by P (Cl), and likewise Se is replaced by As (Br). In sharp contrast to the VI-substitution cases, the averaged phonon frequency is not expected to have a significant drop after substitutions, because the atomic mass after chemical substitutions is close to that of the prototypes. Thus, as the calculations will show below, the changes of $T_c$ follow closely the changes of $\lambda$ in the V- and VII-substitution cases. Note that the absence of imaginary frequency in the phonon spectra, as exhibited in Fig. 3 and Appendix C, ensures the lattice dynamic stabilities for all the cases of interest.

Due to the decrease of valence electrons after V-substitutions, the electronic energy bands shift up a little bit with respect to the Fermi energy (see Appendix B). There are two closely spaced van Hove singularities near the Fermi level that give rise to the sharp peak in the DOS [52]. Thus, the partial substitution of sulfur atoms by phosphorus atoms results in a shift of the Fermi level and the enhancement of the DOS, as summarized in Table I and also seen in Appendix E. It turns out that the DOS increases first and then decreases upon increasing the V-substitution rates. Notably, the DOS can reach very large values, e.g., 10.55 in $H_3S_{0.9}P_{0.1}$ and 8.38 in $H_3Se_{0.85}As_{0.15}$, in units of Hartree$^{-1}$ per spin. Although the phonon spectra hardly change after V-substitutions, the phonon linewidths follow a close trend of the changes in the DOS. The magnitudes of phonon linewidths in the intermediate- and high-frequency regions rise sharply as the P-substitution rate reaches $x = 0.1$ and then fall steeply as the rate further increases to $x = 0.2$, as shown in Figs. 3(a) and 3(b). Thus, the electron-phonon coupling constant $\lambda$ follows the same trend of the changes in the DOS and in the phonon linewidths, as shown in Fig. 2(d). This is because the Hopfield expression for $MgB_2$-type superconductivity [45,46], i.e., $\lambda = N(E_F)D^2/(M\omega^2)$, requires a linear relationship between $\lambda$ and the DOS $N(E_F)$, as studied in Appendix F. Analysis of $\lambda'(\omega)$ plotted in Fig. 2(c) further confirms the enhancement of electron-phonon couplings in the intermediate- and high-frequency regions in $H_3S_{0.9}P_{0.1}$. Very similar behaviors can be found as the As-substitution rate increases from zero to $x = 0.2$ in $H_3Se_{1-x}As_x$, as seen in Figs. 2(c) and 2(d) and Appendix C. We find that the maximal coupling-constant values are 2.12 in $H_3S_{0.9}P_{0.1}$ and 1.97 in $H_3Se_{0.85}As_{0.15}$.

Based on the above results, we use Eq. (1) with $\mu^* = 0.12$ to estimate $T_c$ for the two V-substitution systems, and we plot them in Fig. 2(d). The $T_c$ are found to be as high as 250 K in $H_3S_{0.9}P_{0.1}$ and 185 K in $H_3Se_{0.85}As_{0.15}$, which are greatly enhanced from the 194 K (160 K) in the prototypical $H_3S$ ($H_3Se$). Given the possible variation of the effective Coulomb repulsion $\mu^*$ in the range of 0.1–0.15, the $T_c$ in $H_3S_{0.9}P_{0.1}$ may also vary in the range of 227–265 K.

In the VII-substitution cases we have studied two cases: $H_3S_{1-x}Cl_x$ and $H_3Se_{1-x}Br_x$. In general, the electronic energy bands shift down with respect to the Fermi energy because of the increase of valence electrons; the DOS at the Fermi energy, the phonon linewidths, and hence the electron-phonon coupling constants all decrease monotonously as the degree of VII-substitutions increases. As a consequence, the $T_c$ drops monotonously upon increasing the VII-substitution degree. These results are summarized in Table I, Figs. 2(e) and 2(f), and Appendix C.

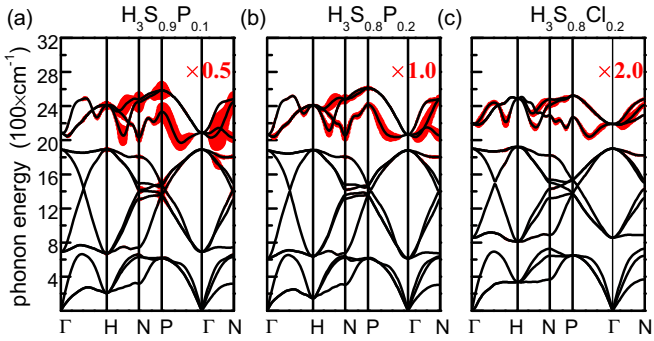


FIG. 3. Phonon spectra with a phonon linewidth of V- and VII-substitution systems at 200 GPa. (a) $H_3S_{0.9}P_{0.1}$, (b) $H_3S_{0.8}P_{0.2}$, and (c) $H_3S_{0.8}Cl_{0.2}$. The magnitude of the phonon linewidths in $H_3S_{0.9}P_{0.1}$ ($H_3S_{0.8}Cl_{0.2}$) is too large (small) and thus plotted with half of (twice) the real values.

## V. THE EFFECT OF PRESSURE

We now take into account the influence of varying the high pressure on the superconductivity [15,16] in the case of $H_3S_{1-x}P_x$. Since we are particularly interested in optimizing the $T_c$, we focus on two cases suggested by Fig. 2(d): $H_3S_{0.9}P_{0.1}$ and $H_3S_{0.925}P_{0.075}$. The main results are summarized in Table II and Fig. 4. In the case of $H_3S_{0.9}P_{0.1}$, the $T_c$ reaches the highest value at 200 GPa and remains the same value up to 225 GPa, whereas in the case of $H_3S_{0.925}P_{0.075}$, the $T_c$ increases monotonously as the pressure rises from 150 to 250 GPa, beyond which a structure instability is found. Results in the latter case follow the fact that the DOS at the Fermi energy, the phonon linewidths, and the electron-phonon coupling constants all increase gradually with increasing pressure. For $\mu^* = 0.1$, the $T_c$ of $H_3S_{0.925}P_{0.075}$ at 250 GPa can reach 280 K. The effect of pressure is similar to those in the H-rich materials [27–32,38], e.g., the predicted $YH_6$ [38] with

TABLE II. Fermi-surface DOS (in units of Hartree$^{-1}$/spin) and electron-phonon coupling constant λ of $H_3S_{1-x}P_x$ under different pressures.

| | $H_3S_{0.925}P_{0.075}$ | | $H_3S_{0.9}P_{0.1}$ | |
|---|---|---|---|---|
| Pressure (GPa) | DOS | λ | DOS | λ |
| 150 | 9.16 | 1.96 | 9.13 | 1.9 |
| 175 | 9.64 | 2.0 | 9.77 | 1.98 |
| 200 | 9.92 | 2.1 | 10.55 | 2.12 |
| 225 | 10.67 | 2.24 | 10.4 | 2.19 |
| 250 | 11.1 | 2.44 | 9.87 | 2.24 |

$T_c = 260$ K. We note that the pressure of 250 GPa has already been feasible in the $H_3S$ experiment by Drozdov *et al.* [16]. Given the range of $\mu^* = 0.1$–$0.15$, the $T_c$ in such an optimized case is at least as high as 241 K, as indicated by the error bar in Fig. 4(c). (For $\mu^* = 0.12$, which yields a $T_c$ of 194 K in $H_3S$, we find $T_c = 264$ K.)

## VI. DISCUSSION

We have investigated the influence of partial atomic substitution on the superconductivity of hydrogen chalcogenides using first-principles calculations with the VCA. Our study has highlighted the key roles of metallized covalent bonds and low atomic mass in boosting the $T_c$ of BCS superconductivity. The former can produce large electron-phonon couplings, whereas the latter can yield high-frequency phonon modes, and in fact the highly compressed $H_3S$ constitutes both advantages. We now take $H_3S$ as the example to summarize our results. In the VI-substitution cases, the reduction of the DOS at Fermi energy dilutes the covalent metallic nature even though the coupling constant can be enhanced in the Te-substitution case, and the $T_c$ is lowered because of the stronger atomic mass. This leads us to further study the cases of Cl- and P-substitutions, in which the atomic mass remains hardly changed. In the P-substitution case, the DOS, the phonon linewidths, the coupling constant, and hence the $T_c$ all increase as the substitution rate increases from zero up to $x = 0.1$. In sharp contrast, the oppose trend occurs in the Cl-substitution case.

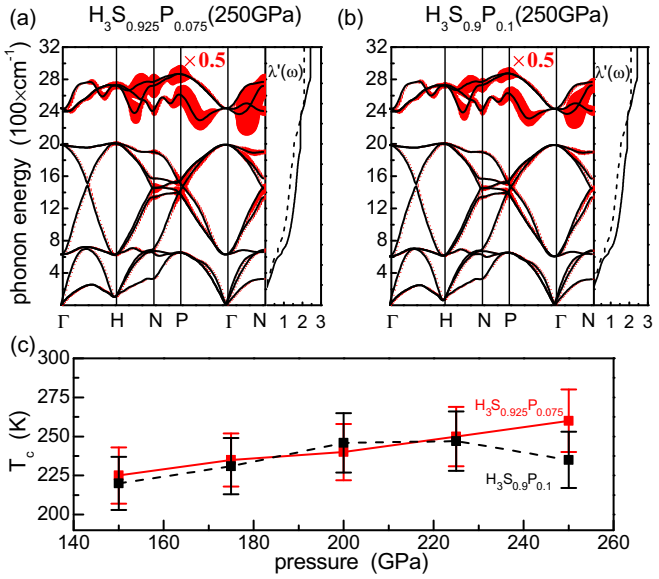


FIG. 4. The effect of pressure in $H_3S_{1-x}P_x$. (a) and (b) The phonon spectra and $\lambda'(\omega)$ of $H_3S_{0.925}P_{0.075}$ and $H_3S_{0.9}P_{0.1}$ at 250 GPa. The magnitude of the phonon linewidth is plotted with half of the real values. The solid (dashed) lines plot $\lambda'(\omega)$ at 250 (200) GPa. (c) $T_c$ of $H_3S_{0.925}P_{0.075}$ (red solid line) and $H_3S_{0.9}P_{0.1}$ (black dashed line) vs pressure. The error bars indicate the value range of $T_c$ with $\mu^* = 0.1$–$0.15$.

In particular, we have shown that in the optimized case of $H_3S_{0.925}P_{0.075}$ the $T_c$ may reach a record high value of 280 K at 250 GPa, which is a feasible pressure in current experiments and would not induce any structure instability. In light of our results, it might be possible that the silicon substitution would also enhance the $T_c$ of a high-pressure $H_3S$ superconductor. Because of the even fewer valence electrons, the optimum $T_c$ of $H_3S_{1-x}Si_x$ might occur at even lower substitution concentration, which might be easier to realize in experiment. For example, we also find $T_c = 274$ K in the case of $H_3S_{0.96}Si_{0.04}$, as shown in Appendix D.

In the future, inclusion of anharmonic effects [19] may improve our predictions and thus better guide the experiments. As shown in the previous work [19], anharmonicity will mainly affect the phonon spectra and corrects the discrepancy between calculations and experiments. In our work, the $T_c$ enhancement is mainly due to the increase of the DOS at the Fermi level when the sulfur atoms are partially substituted by the phosphorus atoms. In addition, the slight change of phonon spectra under the substitution is clearly seen in Fig. 3. Thus, one can simply consider that anharmonicity and phosphorus substitution affect the $T_c$ of $H_3S$ in two independent manners. To focus on the study of increasing $T_c$ due to phosphorus substitution and to directly compare with the experimental observations, we have started from the *ad hoc* case with $T_c = 194$ K in the $H_3S$ case. Nevertheless, our finding is exciting. It not only suggests that partial atomic substitution may lead to possible superconductivity above the ice point in the highly compressed $H_3S$, but it also gives hope that in principle the low atomic mass and strong covalent metallic nature may be designed in novel materials to realize high-$T_c$ BCS superconductivity under ambient pressures.

*Note added.* During the submission of our manuscript, a highly compressed $H_3P$ was experimentally found to be superconducting at 103 K under 207 GPa [72].

## ACKNOWLEDGMENTS

Y.F.G. and Y.G.Y were supported by the NSFC (Grants No. 11225418 and No. 11574029), the MOST Project of China (Grant No. 2014CB920903). F.Z. was supported by UT Dallas research enhancement funds. F.Z. acknowledges the Aspen Center for Physics (NSF Grant No. 1066293 and the Trustee's Fund) for hospitality during the finalization of this work. F.Z. thanks Bing Lv and Anvar Zakhidov for helpful discussions. The computations were performed on TianHe-1(A) at the National Supercomputer Center in Tianjin.

## APPENDIX A: SUPPLEMENTARY METHODS

The microscopic electron-phonon matrix elements $M^{\mathbf{q},\nu}_{i\mathbf{k},j\mathbf{k}+\mathbf{q}}$ describe the electronic scattering from the state with momentum $\mathbf{k}$ to another state $\mathbf{k}+\mathbf{q}$ by a phonon mode $(\mathbf{q}, \nu)$, and they can be expressed as [68–70]

$$M^{\mathbf{q},\nu}_{i\mathbf{k},j\mathbf{k}+\mathbf{q}} = \left(\frac{\hbar}{m^*\omega_{\mathbf{q},\nu}}\right)^{1/2} \langle i,\mathbf{k}|\delta^{\mathbf{q},\nu}V|j,\mathbf{k}+\mathbf{q}\rangle, \quad \text{(A1)}$$

where $m^*$ is the atomic mass and $\delta^{\mathbf{q},\nu}$V is the derivative of the self-consistent effective potential with respect to atomic displacement associated with the phonon mode $(\mathbf{q}, \nu)$ of frequency $\omega_{\mathbf{q},\nu}$. It follows that the Eliashberg function reads

$$\begin{aligned}\alpha^2\mathrm{F}(\omega) &= \frac{1}{\hbar N(E_F)}\sum_{\mathbf{q}},\nu\delta(\omega-\omega_{\mathbf{q},\nu}) \\ &\quad\times\sum_{i,j,\mathbf{k}}\left|M^{\nu}_{i\mathbf{k},j\mathbf{k}+\mathbf{q}}\right|^2\delta(\epsilon_{i\mathbf{k}}-\epsilon_F)\delta(\epsilon_{j\mathbf{k}+\mathbf{q}}-\epsilon_F) \\ &= \sum_{\mathbf{q},\nu}\frac{\gamma_{\mathbf{q},\nu}}{4\pi\omega_{\mathbf{q},\nu}N(E_F)}\delta(\omega-\omega_{\mathbf{q},\nu}), \quad \text{(A2)}\end{aligned}$$

where $\epsilon_{i\mathbf{k}}$ is the band energy of the Bloch state $|i,\mathbf{k}\rangle$, $N(E_F)$ is the DOS at the Fermi energy, and $\gamma_{\mathbf{q},\nu}$ indicates the phonon linewidth. Moreover, $T_c$ is thus estimated by the Allen-Dynes-modified McMillan formula [50],

$$T_c = f_1 f_2 \frac{\langle\omega\rangle_{\log}}{1.2}\exp\left[-\frac{1.04(1+\lambda)}{\lambda-\mu^*(1+0.62\lambda)}\right], \quad \text{(A3)}$$

where $f_1$ and $f_2$ are defined as

$$\begin{aligned} f_1 &= \left\{1+\left[\frac{\lambda}{2.46(1+3.8)\mu^*}\right]^{3/2}\right\}^{1/3}, \\ f_2 &= 1+\frac{(\omega_2/\langle\omega\rangle_{\log}-1)\lambda^2}{\lambda^2+[1.82(1+6.3\mu^*)(\omega_2/\langle\omega\rangle_{\log})]^2}. \end{aligned} \quad \text{(A4)}$$

These two functions are required to be unity for the weak electron-phonon coupling [50]. $\langle\omega\rangle_{\log}$ and $\omega_2$ are defined as

$$\begin{aligned}\langle\omega\rangle_{\log} &= \exp\left[\frac{2}{\lambda}\int_0^\infty \alpha^2\mathrm{F}(\omega)\log\omega\frac{d\omega}{\omega}\right], \\ \omega_2 &= \left[\frac{2}{\lambda}\int_0^\infty \omega\alpha^2\mathrm{F}(\omega)d\omega\right]^{1/2}, \end{aligned} \quad \text{(A5)}$$

which represent the logarithmically averaged phonon frequency and the second moment of the normalized weight function, respectively.

## APPENDIX B: ELECTRONIC BAND STRUCTURES OF V-, VI-, AND VII-SUBSTITUTION SYSTEMS

In Fig. 5, we show the electronic band structures of several representative VI-substitution systems. By comparing the band structures of VI-substitution systems (black solid lines) and that of $H_3S$ (red dashed lines), we find that VI substitution mainly affects the bands near the Γ point.

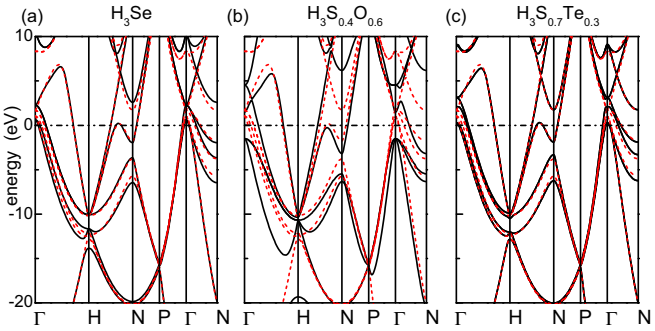


FIG. 5. Electronic band structures of VI-substitution systems at 200 GPa. (a) $H_3Se$, (b) $H_3S_{0.4}O_{0.6}$, and (c) $H_3S_{0.7}Te_{0.3}$. For comparison, the red dashed lines show the band structure of $H_3S$. The Fermi energies are set to be zero.

In Fig. 6, we show the electronic band structures of several representative V-substitution and VII-substitution systems. By comparing the band structures of substitution systems (black solid lines) and that of $H_3S$ or $H_3Se$ (red dashed lines), clearly for V-substitution systems the Fermi energies shift down slightly versus that of $H_3S$ or $H_3Se$, whereas for VII-substitution systems the Fermi energies shift up slightly. Other effects are almost invisible.

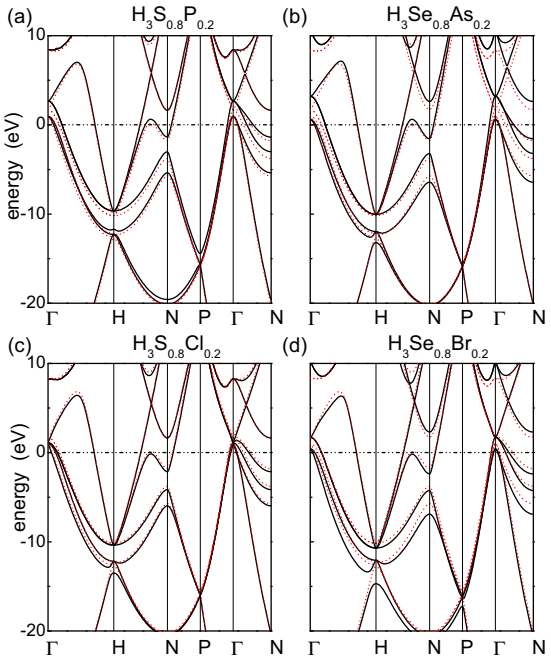


FIG. 6. Electronic band structures of V-substitution and VII-substitution systems at 200 GPa. (a) $H_3S_{0.8}P_{0.2}$, (b) $H_3Se_{0.8}As_{0.2}$, (c) $H_3S_{0.8}Cl_{0.2}$, and (d) $H_3Se_{0.8}Br_{0.2}$. For comparison, the red dashed lines show the band structure of $H_3S$ in (a) and (c) and that of $H_3Se$ in (b) and (d). The Fermi energies are set to be zero.

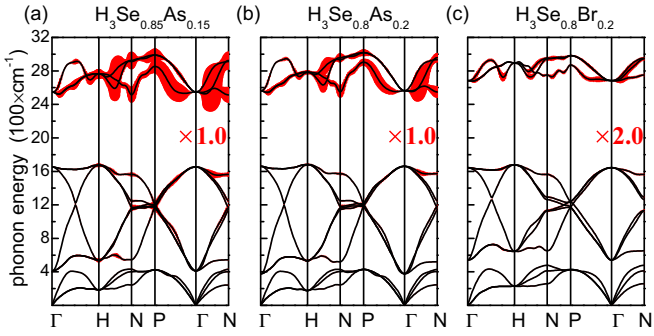


FIG. 7. Phonon spectra and linewidths of V-substitution and VII-substitution systems at 200 GPa. (a) $H_3Se_{0.85}As_{0.15}$, (b) $H_3Se_{0.8}As_{0.2}$, and (c) $H_3Se_{0.8}Br_{0.2}$. The magnitude of the phonon linewidths in $H_3Se_{0.8}Br_{0.2}$ is too small and thus plotted with twice of the real values.

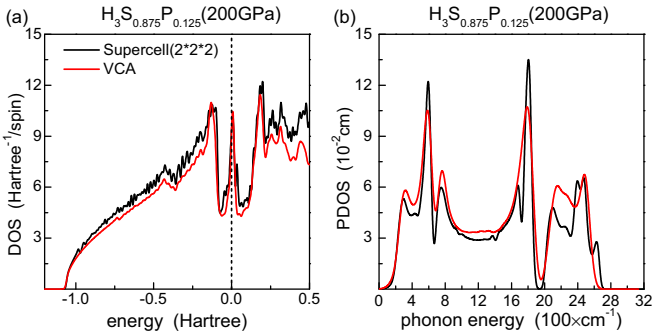


FIG. 9. Comparison between the results obtained by the supercell method and by the VCA. (a) Electron DOS and (b) phonon DOS in $H_3S_{0.875}P_{0.125}$ at 200 GPa. Note that in $H_3S$, the position of the DOS peak is lower than the Fermi level.

## APPENDIX C: PHONON SPECTRA AND LINEWIDTHS OF V- AND VII-SUBSTITUTION SYSTEMS

In Fig. 7, we show our calculation results of the phonon spectra and phonon linewidths for several representative V-substitution and VII-substitution systems.

## APPENDIX D: CALCULATIONS FOR ONE CASE OF SILICON SUBSTITUTION

For the silicon-substitution cases, we have performed calculations for the case of $H_3S_{0.96}Si_{0.04}$ at 250 GPa. The phonon spectrum and phonon linewidths of $H_3S_{0.96}Si_{0.04}$ are shown in Fig. 8. The absence of imaginary phonon modes suggests the stability of the considered material in the $Im\bar{3}m$ phase at the considered pressure. In addition, the corresponding DOS and $\lambda$ are found to be 10.93 Hartree$^{-1}$ per spin and 2.56, respectively. Based on the McMillan formula, we further obtain $T_c = 274$ K with $\mu^* = 0.1$.

## APPENDIX E: SUPERCELL METHOD AND THE VCA

To benchmark the validity of the VCA in the present work, we have also performed calculations for $H_3S_{0.875}P_{0.125}$ by using the supercell method, substituting one S atom by one P atom in the $2 \times 2 \times 2$ supercell. The comparison between the two methods is shown in Fig. 9, and their agreement shows the applicability of the VCA to the present work. We note that the results about electron-phonon coupling and superconductivity are not obtained due to the limit of computing power.

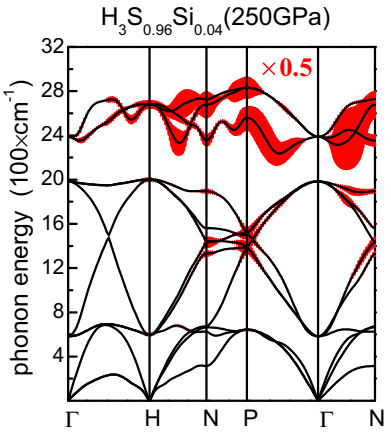


FIG. 8. Phonon spectrum and phonon linewidths of $H_3S_{0.96}Si_{0.04}$ at 250 GPa. The magnitude of the phonon linewidths is too large and thus plotted with half of the real values.

## APPENDIX F: RELATIONSHIP BETWEEN DOS AND λ

The electron-phonon coupling constant can be approximatively written as $\lambda = N(E_F)D^2/(M\omega^2)$, which is the Hopfield expression for $MgB_2$-type superconductivity [45]. Here $D$ is the deformation potential, $M$ is the effective mass, and $\omega$ is the phonon frequency. In the present work, the $T_c$ enhancement is mainly due to the increase of the DOS at Fermi level $N(E_F)$, when the sulfur atoms are partially substituted by the phosphorus atoms; there is hardly any change in the phonon spectrum. Therefore, $\lambda$ scales linearly with the DOS $N(E_F)$, as shown in Fig. 10.

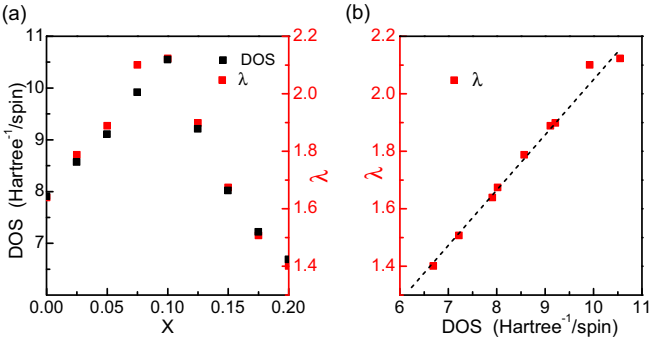


FIG. 10. The electronic DOS and the electron-phonon coupling $\lambda$ in $H_3S_{1-x}P_x$. (a) DOS and $\lambda$ vs the substitution concentration. (b) Linear relationship between $\lambda$ and DOS.

[1] D. Delft and P. Kes, Phys. Today **63**(9), 38 (2010).
[2] J. Bardeen, L. N. Cooper, and J. R. Schrieffer, Phys. Rev. **108**, 1175 (1957).
[3] J. Nagamatsu, N. Nakagawa, T. Muranaka, Y. Zenitani, and J. Akimitsu, Nature (London) **410**, 63 (2001).
[4] S. L. Bud'ko, G. Lapertot, C. Petrovic, C. E. Cunningham, N. Anderson, and P. C. Canfield, Phys. Rev. Lett. **86**, 1877 (2001).
[5] V. L. Ginzburg and D. A. Kirzhnits, *Problemy Vysokotemperaturnoy Sverkhprovodimosti* (Nauka, Moscow, 1977) [English translation: *High-Temperature Superconductivity* (Consultants Bureau, New York, 1982)].
[6] J. G. Bednorz and K. A. Müller, Z. Phys. B **64**, 189 (1986).
[7] M. K. Wu, J. R. Ashburn, C. J. Torng, P. H. Hor, R. L. Meng, L. Gao, Z. J. Huang, Y. Q. Wang, and C. W. Chu, Phys. Rev. Lett. **58**, 908 (1987).
[8] A. Schilling, M. Cantoni, J. D. Guo, and H. R. Ott, Nature (London) **363**, 56 (1993).
[9] L. Gao, Y. Y. Xue, F. Chen, Q. Xiong, R. L. Meng, D. Ramirez, C. W. Chu, J. H. Eggert, and H. K. Mao, Phys. Rev. B **50**, 4260(R) (1994).
[10] Y. Kamihara, T. Watanabe, M. Hirano, and H. Hosono, J. Am. Chem. Soc. **130**, 3296 (2008).
[11] Z.-A. Ren, W. Lu, J. Yang, W. Yi, X.-L. Shen, C. Zheng, G.-C. Che, X.-L. Dong, L.-L. Sun, F. Zhou, and Z.-X. Zhao, Chin. Phys. Lett. **25**, 2215 (2008).
[12] G. Wu, Y. L. Xie, H. Chen, M. Zhong, R. H. Liu, B. C. Shi, Q. J. Li, X. F. Wang, T. Wu, Y. J. Yan, J. J. Ying, and X. H. Chen, J. Phys.: Condens. Matter **21**, 142203 (2009).
[13] Y. Li, J. Hao, H. Liu, Y. Li, and Y. Ma, J. Chem. Phys. **140**, 174712 (2014).
[14] D. Duan, Y. Liu, F. Tian, D. Li, X. Huang, Z. Zhao, H. Yu, B. Liu, W. Tian, and T. Cui, Sci. Rep. **4**, 6968 (2014).
[15] A. P. Drozdov, M. I. Eremets, and I. A. Troyan, arXiv:1412.0460.
[16] A. P. Drozdov, M. I. Eremets, I. A. Troyan, V. Ksenofontov, and S. I. Shylin, Nature (London) **525**, 73 (2015).
[17] N. Bernstein, C. S. Hellberg, M. D. Johannes, I. I. Mazin, and M. J. Mehl, Phys. Rev. B **91**, 060511(R) (2015).
[18] D. Duan, X. Huang, F. Tian, D. Li, H. Yu, Y. Liu, Y. Ma, B. Liu, and T. Cui, Phys. Rev. B **91**, 180502(R) (2015).
[19] I. Errea, M. Calandra, C. J. Pickard, J. Nelson, R. J. Needs, Y. Li, H. Liu, Y. Zhang, Y. Ma, and F. Mauri, Phys. Rev. Lett. **114**, 157004 (2015).
[20] D. A. Papaconstantopoulos, B. M. Klein, M. J. Mehl, and W. E. Pickett, Phys. Rev. B **91**, 184511 (2015).
[21] R. Akashi, M. Kawamura, S. Tsuneyuki, Y. Nomura, and R. Arita, Phys. Rev. B **91**, 224513 (2015).
[22] E. J. Nicol and J. P. Carbotte, Phys. Rev. B **91**, 220507(R) (2015).
[23] C. Heil and L. Boeri, Phys. Rev. B **92**, 060508(R) (2015).
[24] J. M. An and W. E. Pickett, Phys. Rev. Lett. **86**, 4366 (2001).
[25] I. I. Mazin and V. P. Antropov, Physica C **385**, 49 (2003).
[26] N. W. Ashcroft, Phys. Rev. Lett. **21**, 1748 (1968).
[27] N. W. Ashcroft, Phys. Rev. Lett. **92**, 187002 (2004).
[28] J. Feng, W. Grochala, T. Jaron, R. Hoffmann, A. Bergara, and N. W. Ashcroft, Phys. Rev. Lett. **96**, 017006 (2006).
[29] J. S. Tse, Y. Yao, and K. Tanaka, Phys. Rev. Lett. **98**, 117004 (2007).
[30] P. Cudazzo, G. Profeta, A. Sanna, A. Floris, A. Continenza, S. Massidda, and E. K. U. Gross, Phys. Rev. Lett. **100**, 257001 (2008).
[31] G. Gao, A. R. Oganov, A. Bergara, M. Martinez-Canales, T. Cui, T. Iitaka, Y. Ma, and G. Zou, Phys. Rev. Lett. **101**, 107002 (2008).
[32] M. I. Eremets, I. A. Trojan, S. A. Medvedev, J. S. Tse, and Y. Yao, Science **319**, 1506 (2008).
[33] E. Zurek, R. Hoffmann, N. W. Ashcroft, A. R. Oganov, and A. O. Lyakhov, Proc. Natl. Acad. Sci. (USA) **106**, 17640 (2009).
[34] D. Y. Kim, R. H. Scheicher, H.-K. Mao, T. W. Kang, and R. Ahuja, Proc. Natl. Acad. Sci. (USA) **107**, 2793 (2010).
[35] D. Y. Kim, R. H. Scheicher, C. J. Pickard, R. J. Needs, and R. Ahuja, Phys. Rev. Lett. **107**, 117002 (2011).
[36] J. A. Flores-Livas, M. Amsler, T. J. Lenosky, L. Lehtovaara, S. Botti, M. A. L. Marques, and S. Goedecker, Phys. Rev. Lett. **108**, 117004 (2012).
[37] H. Wang, J. S. Tse, K. Tanaka, T. Iitaka, and Y. Ma, Proc. Natl. Acad. Sci. (USA) **109**, 6463 (2012).
[38] Y. W. Li *et al.*, Sci. Rep. **5**, 09948 (2015).
[39] R. J. Cava, A. W. Hewat, E. A. Hewat, B. Batlogg, M. Marezio, K. M. Rabe, J. J. Krajewski, W. F. Peck Jr., and L. W. Rupp Jr., Physica C **165**, 419 (1990).
[40] E. A. Ekimov, V. A. Sidorov, E. D. Bauer, N. N. Mel'nik, N. J. Curro, J. D. Thompson, and S. M. Stishov, Nature (London) **428**, 542 (2004).
[41] K. Sasmal, B. Lv, B. Lorenz, A. M. Guloy, F. Chen, Y.-Y. Xue, and C.-W. Chu, Phys. Rev. Lett. **101**, 107007 (2008).
[42] S. A. J. Kimber, A. Kreyssig, Y.-Z. Zhang, H. O. Jeschke, R. Valentí, F. Yokaichiya, E. Colombier, J. Yan, T. C. Hansen, T. Chatterji, R. J. McQueeney, P. C. Canfield, A. I. Goldman, and D. N. Argyriou, Nat. Mater. **8**, 471 (2009).
[43] L. Nordheim, Ann. Phys. **401**, 607 (1931).
[44] H. Rosner, A. Kitaigorodsky, and W. E. Pickett, Phys. Rev. Lett. **88**, 127001 (2002).
[45] L. Boeri, J. Kortus, and O. K. Andersen, Phys. Rev. Lett. **93**, 237002 (2004).
[46] K.-W. Lee and W. E. Pickett, Phys. Rev. Lett. **93**, 237003 (2004).
[47] S. Blackburn, M. Côté, S. G. Louie, and M. L. Cohen, Phys. Rev. B **84**, 104506 (2011).
[48] M. Einaga, M. Sakata, T. Ishikawa, K. Shimizu, M. I. Eremets, A. P. Drozdov, I. A. Troyan, N. Hirao, and Y. Ohishi, Nat. Phys. (2016).
[49] P. B. Allen and B. Mitrović, Solid State Phys. **37**, 1 (1983).
[50] P. B. Allen and R. C. Dynes, Phys. Rev. B **12**, 905 (1975).
[51] A. P. Durajski, R. Szcześniak, and Y. Li, Physica C **515**, 1 (2015).
[52] Y. Quan and W. E. Pickett, Phys. Rev. B **93**, 104526 (2016).
[53] L. Bellaiche and D. Vanderbilt, Phys. Rev. B **61**, 7877 (2000).
[54] A. Sani, B. Noheda, I. A. Kornev, L. Bellaiche, P. Bouvier, and J. Kreisel, Phys. Rev. B **69**, 020105(R) (2004).
[55] S. A. Shevlin, A. Curioni, and W. Andreoni, Phys. Rev. Lett. **94**, 146401 (2005).
[56] D. J. Priour, Jr., E. H. Hwang, and S. Das Sarma, Phys. Rev. Lett. **95**, 037201 (2005).
[57] B. Barbiellini and T. Jarlborg, Phys. Rev. Lett. **101**, 157002 (2008).
[58] J. Noffsinger, S. G. Louie, M. L. Cohen, and F. Giustino, Phys. Rev. Lett. **102**, 147003 (2009).

[59] X. Gonze, Phys. Rev. B **55**, 10337 (1997).
[60] X. Gonze and C. Lee, Phys. Rev. B **55**, 10355 (1997).
[61] X. Gonze, G.-M. Rignanese, M. Verstraete, J.-M. Beuken, Y. Pouillon, R. Caracas, F. Jollet, M. Torrent, G. Zerah, M. Mikami, P. Ghosez, M. Veithen, J.-Y. Raty, V. Olevano, F. Bruneval, L. Reining, R. Godby, G. Onida, D. R. Hamann, and D. C. Allan, Z. Kristallogr. **220**, 558 (2005).
[62] X. Gonze, B. Amadon, P.-M. Anglade, J.-M. Beuken, F. Bottin, P. Boulanger, F. Bruneval, D. Caliste, R. Caracas, M. Côté, T. Deutsch, L. Genovese, Ph. Ghosez, M. Giantomassi, S. Goedecker, D. R. Hamann, P. Hermet, F. Jollet, G. Jomard, S. Leroux, M. Mancini, S. Mazevet, M. J. T. Oliveira, G. Onida, Y. Pouillon, T. Rangel, G.-M. Rignanese, D. Sangalli, R. Shaltaf, M. Torrent, M. J. Verstraete, G. Zerah, and J. W. Zwanziger, Comput. Phys. Commun. **180**, 2582 (2009).
[63] C. Hartwigsen, S. Goedecker, and J. Hutter, Phys. Rev. B **58**, 3641 (1998).
[64] J. A. Flores-Livas, A. Sanna, and E. K. U. Gross, Eur. Phys. J. B **89**, 63 (2016).
[65] S. Zhang, Y. Wang, J. Zhang, H. Liu, X. Zhong, H.-F. Song, G. Yang, L. Zhang, and Y. Ma, Sci. Rep. **5**, 15433 (2015).
[66] M. Komelj and H. Krakauer, Phys. Rev. B **92**, 205125 (2015).
[67] X. Zhong, H. Wang, J. Zhang, H. Liu, S. Zhang, H.-F. Song, G. Yang, L. Zhang, and Y. Ma, Phys. Rev. Lett. **116**, 057002 (2016).
[68] W. L. McMillan, Phys. Rev. **167**, 331 (1968).
[69] P. B. Allen, Phys. Rev. B **6**, 2577 (1972).
[70] P. B. Allen and R. Silberglitt, Phys. Rev. B **9**, 4733 (1974).
[71] *The Electron-Phonon Interaction in Metals*, Selected Topics in Solid State Physics Vol. 16, edited by E. P. Wohlfahrt (North-Holland, Amsterdam, 1981).
[72] A. P. Drozdov, M. I. Eremets, and I. A. Troyan, arXiv:1508.06224.